Research article

Xiaozhuo Qi, Tsz Wing Lo, Di Liu, Lantian Feng, Yang Chen, Yunkun Wu, Hongliang Ren, Guang-Can Guo, Dangyuan Lei* and Xifeng Ren*

Effects of gap thickness and emitter location on the photoluminescence enhancement of monolayer MoS_2 in a plasmonic nanoparticle-film coupled system

https://doi.org/10.1515/nanoph-2020-0178
Received March 8, 2020; accepted April 20, 2020

Abstract: Plasmonic nanocavities comprised of metal film-coupled nanoparticles have emerged as a versatile nanophotonic platform benefiting from their ultrasmall mode volume and large Purcell factors. In the weak-coupling regime, the particle-film gap thickness affects the photoluminescence (PL) of quantum emitters sandwiched therein. Here, we investigated the Purcell effect-enhanced PL of monolayer MoS_2 inserted in the gap of a gold nanoparticle (AuNP)–alumina (Al_2O_3)–gold film (Au Film) structure. Under confocal illumination by a 532 nm CW laser, we observed a 7-fold PL peak intensity enhancement for the cavity-sandwiched MoS_2 at an optimal Al_2O_3 thickness of 5 nm, corresponding to a local PL enhancement of ~350 by normalizing the actual illumination area to the cavity's effective near-field enhancement area. Full-wave simulations reveal a counterintuitive fact that radiation enhancement comes from the non-central area of the cavity rather than the cavity center. By scanning an electric dipole across the nanocavity, we obtained an average radiation enhancement factor of about 65 for an Al_2O_3 spacer thickness of 4 nm, agreeing well with the experimental thickness and indicating further PL enhancement optimization. Our results indicate the importance of configuration optimization, emitter location and excitation condition when using such plasmonic nanocavities to modulate the radiation properties of quantum emitters.

Keywords: nanoparticle-film coupled system; photoluminescence enhancement; plasmonic nanocavity; transition-metal dichalcogenides.

1 Introduction

Transition-metal dichalcogenides (TMDs) [1], as an exceptional class of two-dimensional (2D) post-graphene materials, have attracted a great deal of attention from both fundamental research and technological applications. Their bandgaps range from 1 to 2 eV [2–4] and change from indirect to direct when the bulk/multi-layer TMDs are exfoliated to monolayers [5]. TMDs-based applications in optics and optoelectronics, such as quantum light sources [6], field-effect transistors [7], photodetectors [8, 9], and flexible optoelectronic diodes [10], have been widely reported. Among various TMDs materials, monolayer molybdenum disulfide (MoS_2) has a direct bandgap of 1.8 eV [11], which gives rises to photoluminescence (PL) at visible wavelengths and is favorable for optical devices. However, the PL quantum efficiency of

Xiaozhuo Qi and Tsz Wing Lo contributed equally to this work.

***Corresponding authors: Dangyuan Lei**, Department of Materials Science and Engineering, City University of Hong Kong, 83 Tat Chee Avenue, Kowloon, Hong Kong, China, E-mail: dangylei@cityu.edu.hk; and **Xifeng Ren**, Key Laboratory of Quantum Information, CAS, University of Science and Technology of China, Hefei, 230026, China; and Synergetic Innovation Center of Quantum Information & Quantum Physics, University of Science and Technology of China, Hefei, Anhui, 230026, China, E-mail: renxf@ustc.edu.cn. https://orcid.org/0000-0002-8963-0193
Xiaozhuo Qi, Di Liu, Lantian Feng, Yang Chen, Yunkun Wu and Guang-Can Guo: Key Laboratory of Quantum Information, CAS, University of Science and Technology of China, Hefei, 230026, China; Synergetic Innovation Center of Quantum Information & Quantum Physics, University of Science and Technology of China, Hefei, Anhui, 230026, China, E-mail: qxz@mail.ustc.edu.cn (X. Qi), dludly@mail.ustc.edu.cn (D. Liu), fenglt@mail.ustc.edu.cn (L. Feng), cy123@mail.ustc.edu.cn (Y. Chen), wuyk123@mail.ustc.edu.cn (Y. Wu), gcguo@ustc.edu.cn (G.C. Guo)
Tsz Wing Lo: Department of Applied Physics, The Hong Kong Polytechnic University, Hung Hom, Kowloon, Hong Kong, China, E-mail: tw-billy.lo@connect.polyu.hk
Hongliang Ren: College of Information Engineering, Zhejiang University of Technology, Hangzhou, 310023, China, E-mail: hlren@zjut.edu.cn

bare monolayer MoS_2 is only about 1% owing to its thickness-limited weak light absorption [12]. Therefore, various photonic approaches such as surface plasmon polaritons (SPPs), which have been widely utilized in nanophotonics [13–15], data storage [13], solar cells [16], metasurface [17], and bio-sensing [18], owing to their great field enhancement and field confinement beyond the optical diffraction limit, have been proposed to enhance the PL emission of monolayer MoS_2.

One of the most common plasmonic configurations used for the PL enhancement of TMDs is metallic nanoparticles, which behave like optical nanoantennas [19–21]. However, the nanoparticle-film coupled plasmonic configuration, e. g., gold nanoparticles on a gold film with a dielectric spacer in between, exhibits a more strongly localized electric field in the gap between the nanoparticle and film [22, 23]. This has been demonstrated in several applications such as chemical reaction detection [24], strong coupling [25, 26], and surface-enhanced Raman scattering of molecules [27–29]. An isotropic metal nanosphere placed on a metal surface, which shows new features such as sensitivity to the polarization of incident light [30], is the simplest nanoparticle-film coupled configuration. In contrast to a number of experimental studies on the different shapes of nanoparticles [31, 32], studies on the thickness of the gap are scarce. However, the thickness of the gap plays an important role in the nanoparticle-film coupled plasmonic configuration, since it affects the density and modes of local confined fields [33, 34]. In recent studies, the gap thickness has been altered by changing the thickness of the spacer, which combines the emitters coupled with the plasmonic configuration. This method makes it impossible to study the coupling effect or the PL enhancement effect with the confined field at a certain position within the gap. A detailed study on the effect of gap thickness in PL enhancement in the nanoparticle-film coupled plasmonic configuration can be performed if a TMDs monolayer is inserted into the gap, which is filled by a dielectric material. Previous studies on SPPs have shown that the plasmonic resonance provides a stronger electric field as the emitter approaches the metallic surface. When the emitter is too close to the metallic surface (below 10 nm), decay via non-radiative channels dominates, which is known as fluorescence quenching [35, 36]. These effects compete in nanoparticle-film coupled plasmonic configurations, depending on the thickness of the dielectric spacer. Thus, a comprehensive study of the effect of the dielectric spacer thickness is required to provide insight into the PL enhancement process using a nanoparticle-film coupled plasmonic configuration.

In this study, we investigated the PL enhancement of monolayer MoS_2 using a gold nanoparticle (AuNP)–aluminum oxide (Al_2O_3)–gold film (AuFilm) coupled nanocavity system, which refers to a configuration with gold nanoparticles on top of a gold film spaced by Al_2O_3. Here, the Al_2O_3 spacer consists of two Al_2O_3 layers with the same thickness (t), in which the monolayer MoS_2 is sandwiched. We measured the PL spectral profile and intensity of monolayer MoS_2 in the coupled system for Al_2O_3 spacer thicknesses of t = 0, 3, 5, and 7 nm and determined an optimal Al_2O_3 layer thickness for obtaining maximum PL intensity enhancement of MoS_2. We performed full-wave electromagnetic simulations to interpret the experimental results through modeling the excitonic emission of MoS_2 as the radiation by an electric dipole located in the same nanocavity, and found that the dipole radiation enhancement comes from the cavity's non-central area because at the cavity center a non-radiative quadrupole plasmon mode is induced at the excitation wavelength. Our study points out that the gap thickness and emitter location influence the Purcell effect of quantum emitters coupled to a plasmonic particle-on-film nanocavity, and is important to the field of plasmon-based fluorescence and Raman spectroscopies.

2 Materials and methods

2.1 Sample preparation

2.1.1 Chemical vapor deposition (CVD) of monolayer: MoS_2 on SiO_2/Si substrate. Monolayer MoS_2 was grown on a SiO_2/Si substrate in a quartz tube furnace at atmospheric pressure by a chemical vapor deposition (CVD) method. The thickness of SiO_2 was 300 nm. Prior to growth, SiO_2/Si substrates were cleaned by sonication in acetone, absolute ethanol, and distilled water for 20 min. The substrates were then placed face-down above the ceramic boat filled with 30 mg of MoO_3, which was placed at the center of the quartz tube. Another ceramic boat filled with sulfur (10 mg) was located upstream of the tube at a distance of 12 cm from the center. After purging the system with ultrahigh-purity argon for 20 min, the furnace was kept at 650 °C for 5 min at a heating rate of 15 °C/min.

2.1.2 Al_2O_3 film deposition and film thickness determination: Alumina film deposition (ALD) is a mild and highly precise technique for the deposition of thin films. All our Al_2O_3 films were deposited by alternating the exposure of H_2O and trimethylaluminum (TMA, $Al(CH_3)_3$) at 120 °C. The deposition cycle consisted of: (1) 10 ms H_2O pulses, (2) 10 s purge time (17 sccm N_2), (3) 15 ms pulses of TMA, and (4) 15 s purge time (17 sccm N_2). The Al_2O_3 film thickness is linear with the number of reaction cycles when the growth conditions remain unchanged. We were able to determine the thickness of the gradually deposited Al_2O_3 film at each step by calibrating the total deposition reaction cycles to the final film thickness. The standard deviation of

surface roughness for the Al_2O_3 layer on top of MoS_2 is about 1.4 nm (1.0 nm from the Au film and 0.4 nm from the Al_2O_3 film).

2.1.3 KOH-based wet transfer: MoS_2 monolayers were transferred from the SiO_2/Si substrate using the wet transfer KOH method. Samples were first spin-coated with PMMA at 2,000 rpm, and then detached in a KOH solution (30%), washed several times in DI water, and transferred onto either bare or Al_2O_3-coated Au films. These samples were then heated up to 180 °C to obtain dry samples. We used acetone to clean the PMMA and blow-dry the sample by clean N_2 from IPA solution.

2.2 Optical characterization: Raman spectroscopy and scanning confocal micro-spectroscopy

To determine the layer number of MoS_2 flakes used in this work, we measured the Raman spectrum of a MoS_2 flake on Si substrate using a confocal Raman spectrometer. Figure S1 displays the Raman spectra of the monolayer MoS_2 that we used. In the Raman spectra, two modes $E1_{2g}$ (in-plane) and A_{1g} (out-of-plane) separated by ~20 cm^{-1} are clearly observed, which is typical for monolayer MoS_2 [37]. To measure the PL spectra of nanocavity-sandwiched monolayer MoS_2 and control sample, we used the experimental setup of the scanning confocal micro-spectroscopy system shown in Figure S2. In this system, a continuous-wave laser at 532 nm is transmitted through a polarizer to produce a linear-polarized beam, which then excites the sample deposited on a three-axis piezo stage through an objective (OLYMPUS, N.A. = 0.9, 100×). The emission from the sample was collected with the same objective and detected with a single photon avalanche diode (SPAD). A dichroic plate was used to block the 532 nm laser and transmit the PL of MoS_2. Here, we use a spatial filtering system that combines two lenses (f = 35 mm) together with a pinhole (25 μm diameter). White light (from a white light source) transmitted through an objective illuminates the sample, enabling the CCD to image it clearly. We obtained the PL map of the sample by scanning it. In addition to this, we also use a spectrograph (Princeton Instruments, Acton SP2500) to obtain the PL spectrum of the sample.

2.3 Numerical simulations

We performed numerical simulations on the AuNP–Al_2O_3–AuFilm coupled system using Lumerical FDTD to obtain a better interpretation of our experimental results obtained earlier [38]. We used two-step calculation to simulate the total emission enhancement of the AuNP–Al_2O_3–AuFilm. The dielectric constant of gold was obtained from Johnson and Christy date [39], and the refractive index of SiO_2 layer was set as 1.5. A total-field scattered-field source at 532 nm was used to excite the 200 nm AuNP on 150 nm AuFilm at normal incidence. In simulation, two orthogonal electric dipoles were set in the gap separately to mimic zero-valley-polarization emissions of monolayer MoS_2 at room temperature. These dipoles were displaced from the center of the particle-film gap to mimic the emissions from multiple dipoles in the monolayer MoS_2. Mesh discretization was set to be 0.5 nm inside the dielectric spacer region and gradually increased outside the sandwiched dielectric region. The total power emitted by the dipole was obtained by integration the Poynting vector of a 3 nm power box surrounding the dipole while the total power radiated outside the nanostructure was obtained by integration the Poynting vector of a 1,000 nm power box surrounding the nanostructure.

3 Result and discussion

As described earlier, we used the CVD method to prepare the monolayer MoS_2 used in the experiment [40–43]. We obtained the reference sample as shown in Figure 1A, by transferring it onto the SiO_2 substrate whose thickness is 300 nm. The sample for the AuNP–AuFilm coupled system is shown in Figure 1D, where a gold film of thickness of 150 nm is deposited between the monolayer MoS_2 and SiO_2 substrate. The AuNP on top of monolayer MoS_2 has a diameter of 200 nm. More details about the sample preparation procedures can be found in the Supplementary Material.

The samples were characterized using the experimental setup described previously. The results are shown in Figure 1. Figure 1B and C are for bare MoS_2 while Figure 1E and F are for the sample with the AuFilm. According to the PL maps in Figure 1B and E, a pronounced PL enhancement of up to six was observed at the position where the AuNP and AuFilm were coupled. We selected the positions with and without AuNPs as indicated by the red arrow and dashed circles in Figure 1B and E, and recorded the corresponding PL spectra, as shown in Figure 1C and F. In Figure 1C, the spectra (black curve) have two peaks located at 680 and 623 nm, which correspond to the A1 and B1 band transitions, respectively, of MoS_2, and are consistent with the measurements for bare MoS_2 in the literature [44]. In Figure 1F, we observe that the PL spectra with AuNPs (red curve) exhibit a significant enhancement at the A1 band, compared to that without AuNPs (blue curve). For simplicity, we used the peaks at the A1 band to characterize the PL enhancement of our samples. We denote the counts at the A1 band as $N_{coupled}$ and N_{film} for the red and blue curves, respectively. Taking into account the dark count N_{dark} of the spectrometer, the PL enhancement factor is defined as $(N_{coupled}\text{-}N_{dark})/(N_{film}\text{-}N_{dark})$. In our case, the value N_{dark} = 600 is obtained by measuring the samples without any excitation laser. It is to be noted that we used the spectra obtained from the same MoS_2 sample (red and blue curves) for a fair comparison, rather than the red and black curves from different MoS_2 samples. In addition to the pronounced peak intensity enhancement, we also observe a clear blue-shift in the PL peak for the nanocavity-sandwiched MoS_2 in comparison to the same MoS_2 flake on the Au film. This may be due to gap plasmon induced dark exciton emission from the sandwiched MoS_2 [45–49].

Using the above definition, we obtained the PL enhancement factor of AuNP–Al_2O_3–AuFilm coupled system for the sample shown in Figure 1D. We now demonstrate the tuning of this PL enhancement factor by introducing dielectric spacers between the MoS_2 and the gold nanostructures. As illustrated in Figure 2A, two layers

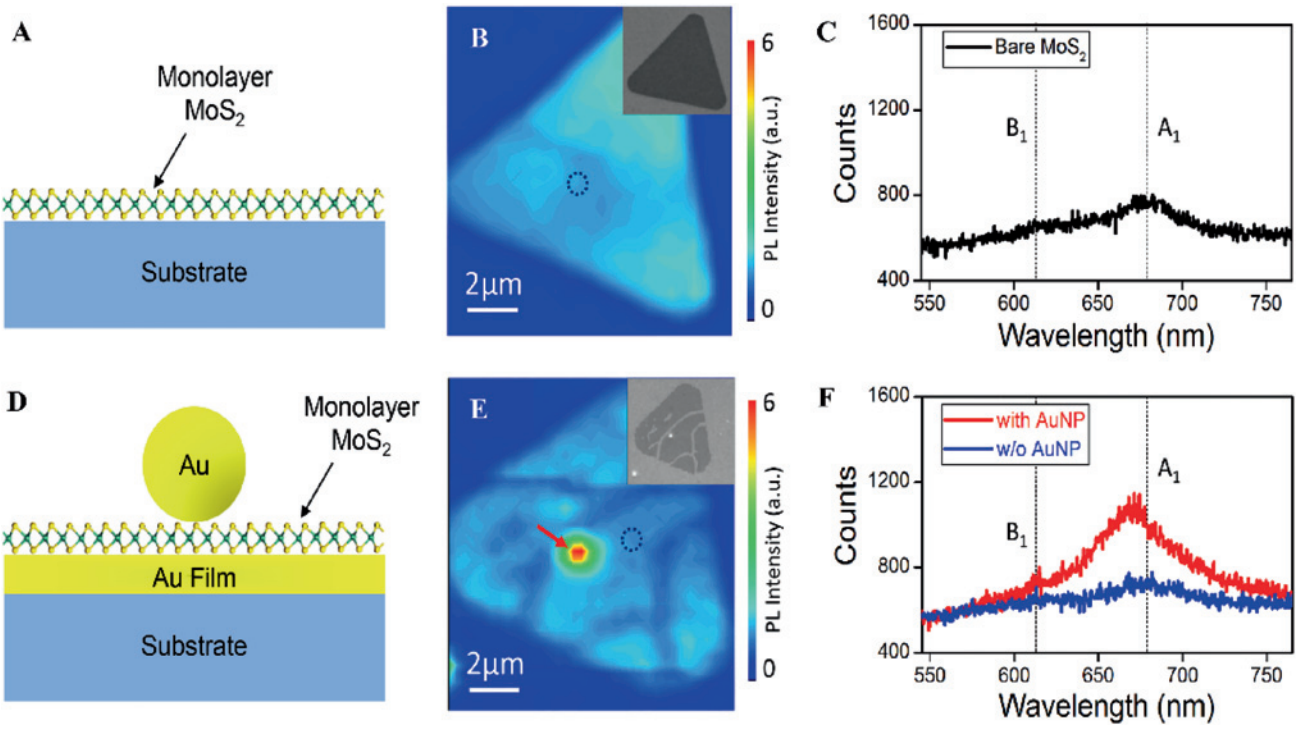

Figure 1: (A) Schematic representation of monolayer MoS_2 on a bare substrate. (B) PL intensity map and SEM image of monolayer MoS_2 on a bare substrate. (C) PL spectra of monolayer MoS_2 in (B) (black dashed circle). (D) Schematic representation of monolayer MoS_2 on AuFilm with AuNP. (E) PL intensity map and SEM image of monolayer MoS_2 with AuNP and AuFilm. (F) PL spectra of monolayer MoS_2 on the AuFilm with and without AuNPs (red and blue curves, respectively), corresponding to (E) (red arrow and black dashed circle, respectively).

of Al_2O_3 with a thickness of t were deposited before and after the monolayer MoS_2 was transferred onto the AuFilm. These formed spacers between MoS_2 and the plasmonic components (i. e., AuFilm and AuNP), modifying the gap between AuFilm and AuNP, and hence, the electric field exciting MoS_2. In Figure 2B–D, the experimentally measured PL for three different samples are displayed, where the thicknesses of the Al_2O_3 spacer are t = 3 nm (Figure 2B), t = 5 nm (Figure 2C), and t = 7 nm (Figure 2D), respectively. The bright spots, which can be found in either the PL maps or the SEM images (as insets), indicate the presence of AuNPs. As before, we selected the areas with (red arrows) and without (black circles) AuNPs, and collected the PL spectra as shown in Figure 2E–G, respectively. Similar to the case where t = 0 (Figure 1F), the PL spectra show overall enhancement when AuNPs are involved. The peak at the A1 band exhibited the best enhancement when t = 5 nm. For t = 3 nm, the field enhancements are comparable for both the A1 and B1 bands, such that the peak at the A1 band is indistinct. As the spacer thickness further increases, the gap between AuNP and AuFilm increases as well, resulting in a weaker electric field that excites the MoS_2. Figure S3 shows experimentally-measured results of other samples.

According to the definition of the PL enhancement factor in section 2, we extracted the PL enhancement factors at the A1 band for different spacer thicknesses, as shown in Figure 3. Using the same thickness for four samples, the average PL enhancement factors determined are 4.38 for t = 0 nm, 6.89 for t = 3 nm, 7.74 for t = 5 nm and 2.22 for t = 7 nm, respectively. Thus, the enhancement effect of the AuNP–Al_2O_3–AuFilm coupled system is optimal when the thickness of the Al_2O_3 spacer is 5 nm. We reorganized the enhancement factors of the intensity of the PL maps and the enhancement factors of the spectra peaks in Figure S4. The average PL emission counts of the t = 3 nm samples was higher than other samples, because of the broad spectra enhancement.

Figure 4A displays the schematic diagram of the AuNP–Al_2O_3–AuFilm with the Al_2O_3 spacer thickness varying from 2 to 12 nm. For simplicity, monolayer MoS_2 is regarded as a dielectric layer with a thickness of 1 nm in the simulations [11]. Thus, the total spacer thickness varies from 3 to 13 nm. An in-plane dipole with parallel or perpendicular polarization from the displace axis is used to represent the excitonic emission of the MoS_2 monolayer. In our experiment, the 532 nm pump light was focused on the sample after passing through the objective lens. Since the

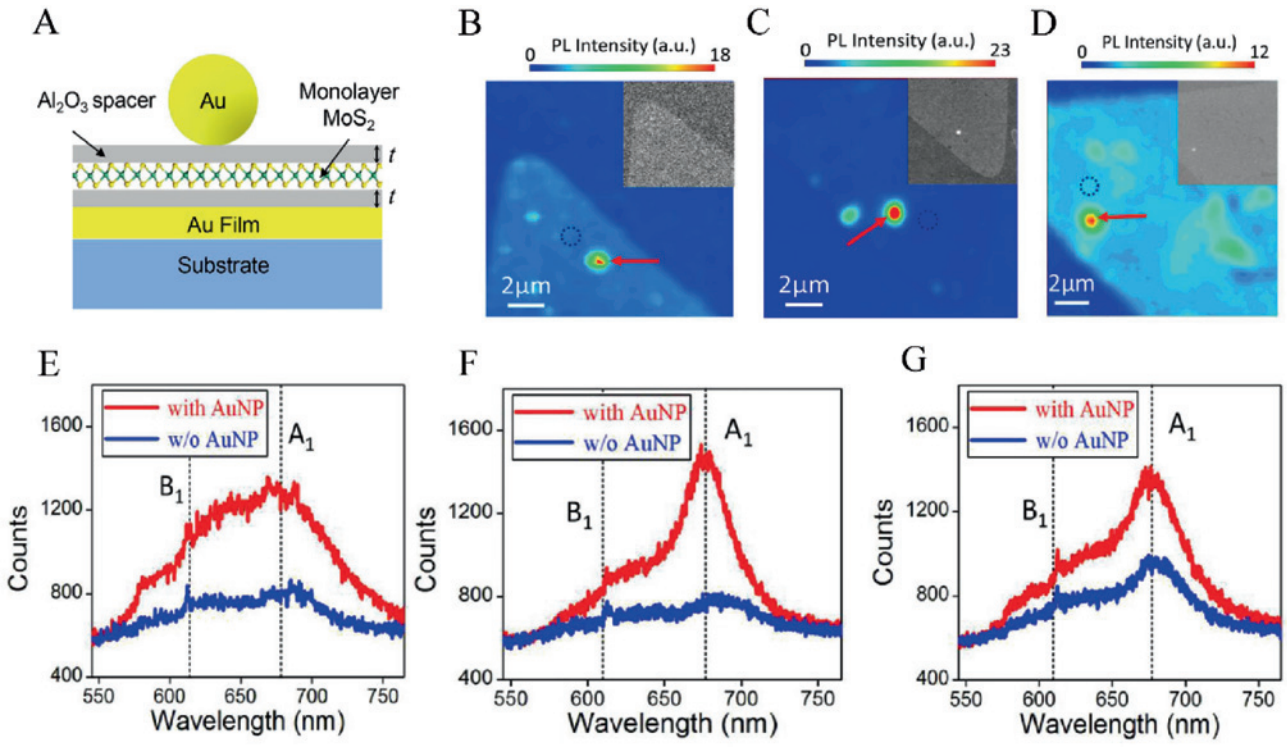

Figure 2: (A) Schematic representation of AuNP–AuFilm coupled system with Al_2O_3 spacers. (B–D) PL intensity maps of monolayer MoS_2 samples. Insets: SEM image of each sample type. The thickness of the spacer is (B) 3 nm (C) 5 nm (D) 7 nm. (E–G) PL spectra of monolayer MoS_2 with and without AuNPs (red and blue curves), corresponding to the position in (B–D) (red arrow and black dashed circle, respectively).

excitonic response in monolayer MoS_2 is more sensitive to the in-plane electric component, we focus on the electric field component Ex and also approximate the 532 nm Gaussian excitation as a simple plane wave at normal incidence. In the 532 nm excitation, the charge distribution is dominated by the transverse mode in the AuNP–AuFilm system, as shown in Figure 4B. The charge distribution confined in the gap is highly similar to an electric quadrupole, which forms two hot spots in the TMDC monolayer. The two hot spots, which are dominated by out-of-plane field component, show antiphase oscillation (Figure 4C). When the gap broadens, the localized electric field enhancement is weakened (Figure 4D) due to the reduced coupling with the image charge in the gold film substrate. We first consider both the orthogonal in-plane dipoles to contribute equally to the enhancement of excitonic emission in the Au-NP film as the degree of valley polarization is insignificant at room temperature. In addition, the enhancement of excitonic emissions along the spectra is simplified by considering the enhancement of emission at 650 nm only because this wavelength lies between the A and B exciton emissions. The quantum efficiency of MoS_2 is assumed to be approximately 1% [12]. As shown in Figure 4E, the enhancement of the in-plane dipole is the weakest when the thickness of the spacer is the smallest. It increases as the spacer widens until it saturates at approximately 9 nm. This could originate from the charging from the quadrupole mode into the transverse dipole mode during the

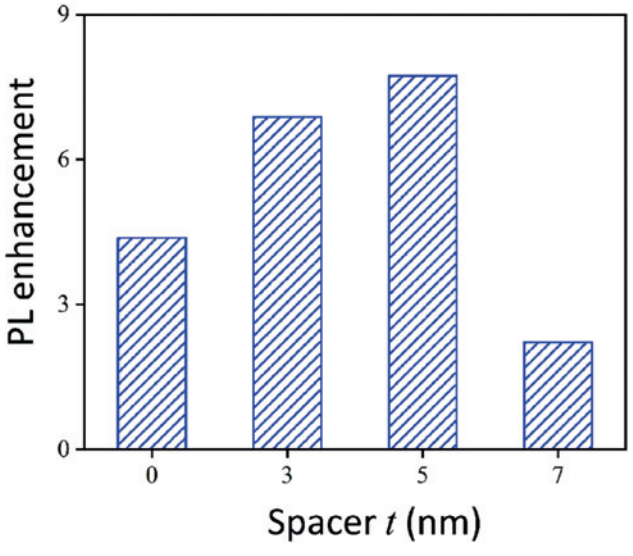

Figure 3: PL enhancement factors for the spectra at the A1 bands using different spacer thicknesses. The thickness of the Al_2O_3 spacer was 0, 3, 5, and 7 nm.

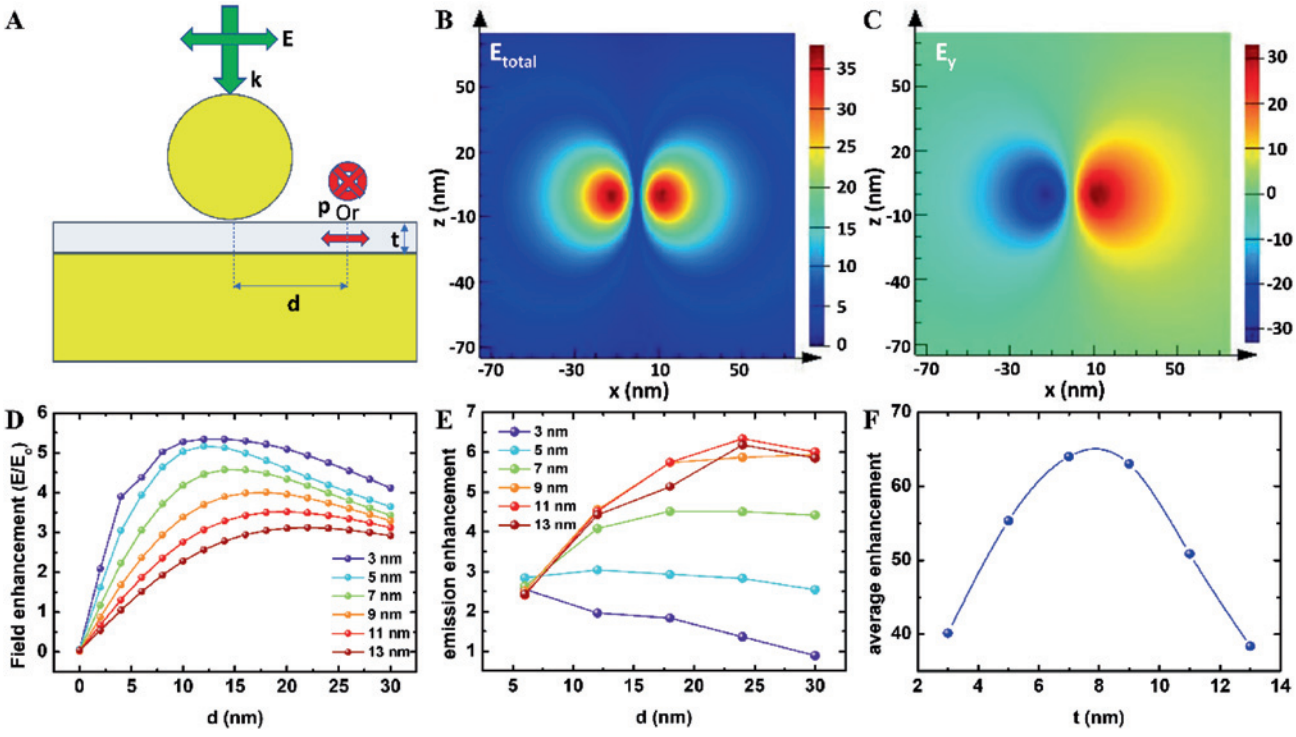

Figure 4: (A) Schematic diagram of AuNP–AuFilm simulation, green arrows indicate the direction of excitation and polarization of the 532 nm laser, while red arrows indicate electric dipole polarization. (B) Near-field distribution of the middle region of the dielectric spacer at 532 nm excitation. (C) Near-field distribution of the out-of-plane field component. (D) Local field amplitude enhancement at 532 nm. (E) Dipole emission enhancement at 650 nm. (F) Average emission enhancement of the AuNP–spacer-AuFilm system as a function of spacer thicknesses.

transition of the gap thickness. To understand the detailed mode distribution at the excitation wavelength, the in-plane view of mode distribution is also shown in Figure S5, which reveals that both the electric field x-component (Figure S5a) and the y-component (Figure S5c) for the 3 nm spacer thickness demonstrate more complex distribution patterns than that for the 13 nm spacer thickness (Figure S5b and d) due to the stronger mode hybridization in the former system. As a result, the average enhancement along the displace axis is maximized when the spacer is approximately 8 nm wide (Figure 4F), which is consistent with the experimentally observed result. Although the above simulation focuses only on the line distribution of emission enhancement rather than the total enhancement, it provides a good agreement with the experimental result. It was calculated that the effective radius of near-field enhancement is 30 nm and the area of effective near-field enhancement is ~2.8×10^{-3} μm^2 from the simulation results [50]. Theoretically, the focused laser spot radius is about 200 nm and the actual illumination area is ~0.126 μm^2. Because the actual illumination area is much larger than the effective plasmonic near-field enhancement area, the plasmon-induced PL intensity enhancement factor should be adjusted accordingly [22]. In our work, the adjusted PL enhancement factor is about 350 for t = 5 nm.

A comprehensive comparison of the experiment and numerical simulations showed that coupling hybridized modes did not enhance PL spectra as the charge distribution in the quadrupole mode. When t = 3 nm in the experiment, the enhancement is not as remarkable as the deformation of the spectra (see Figure 2E). Therefore, even though the 3 nm thickness spacer provides a stronger localized electric field enhancement, the actual enhancement effect is not ideal in the AuNP–Al_2O_3–AuFilm coupled system. The electric field confined results from the hybridized mode, which is influenced by the charge distribution mode. This is possibly related to the in-plane polarization properties of TMD materials. In a weak coupling system, choosing an appropriate confined electric field mode is more beneficial for the efficient enhancement of the desired spectra profile. We also consider possible factors leading to the slight deviation between the simulated and experimental optimal spacer thicknesses. The AuNP–Al_2O_3–AuFilm coupled system in the numerical simulation is idealized as a perfect Au nanosphere sitting on a perfectly flat Au film separated by two smooth Al_2O_3 layers. This assumption deviates from the actual experimental conditions. The colloidal Au nanoparticle used in the experiment could have small facets supporting more complex resonance modes such as cavity

modes that hybridize with both the transverse and gap plasmon modes [31, 51]. Meanwhile, the surface roughness of Au and Al_2O_3 films might induce irregular features in the particle-film gap and local strain in MoS_2 [52], which both can affect the PL enhancement and the intrinsic quantum efficiency of MoS_2.

4 Conclusion

We studied the PL spectral enhancement of monolayer MoS_2 sandwiched in an AuNP–Al_2O_3–AuFilm coupled nanocavity by systematically changing the Al_2O_3 spacer thickness (i. e., the cavity gap thickness). Our experiment shows that a tightly confined electric field does not always enhance the PL spectra sharply. We determined the optimal thickness (t) of the Al_2O_3 spacer to be 5 nm. In our experiment, the AuNP–AuFilm coupled system with a 5 nm spacer can enhance the spectral peak of MoS_2 PL 7.74 fold and the PL intensity 347 fold. Systematic numerical calculations reveal that the average enhancement of the system reaches its maximum at a thickness of approximately 4 nm, which could be due to the influence of the charge distribution mode. These results could be widely used in Purcell enhancement experiments with such plasmonic particle-on-film nanocavities to enhance the emission properties of quantum emitters. Our plasmonic nanocavities can also be used to control the emission properties of more general 2D materials [53] and other dual-resonant optical materials [54, 55].

Acknowledgments: This research was supported by the National Key R & D Program (No. 2016YFA0301700), the National Natural Science Foundation of China (NSFC) (Nos. 61590932, 11774333), the Research Grants Council of Hong Kong (GRF Grant No. 15303718), the Anhui Initiative in Quantum Information Technologies (No. AHY130300), and the Strategic Priority Research Program of the Chinese Academy of Sciences (No. XDB24030601). This work was partially carried out at the USTC Center for Micro and Nanoscale Research and Fabrication.

References

[1] G. Fiori, F. Bonaccorso, G. Iannaccone, et al., "Electronics based on two-dimensional materials," *Nat. Nanotechnol.*, vol. 9, pp. 768–799, 2014, https://doi.org/10.1038/nnano.2014.207.

[2] F. Schedin, A. Geim, S. Morozov, et al., "Detection of individual gas molecules adsorbed on graphene," *Nat. Mater.*, vol. 6, pp. 652–655, 2007, https://doi.org/10.1038/nmat1967.

[3] Q. H. Wang, K. Kalantar-Zadeh, A. Kis, N. J. Coleman, and M. S. Strano, "Electronics and optoelectronics of two-dimensional transition metal dichalcogenides," *Nat. Nanotechnol.* vol. 7, pp. 699–712, 2012, https://doi.org/10.1038/nnano.2012.193.

[4] D. Jariwala, V. K. Sangwan, L. J. Lauhon, T. J. Marks, and M. C. Hersam, "Emerging device applications for semiconducting two-dimensional transition metal dichalcogenides," *ACS Nano*, vol. 8, pp. 1102–1120, 2014, https://doi.org/10.1021/nn500064s.

[5] K. F. Mak, C. Lee, J. Hone, J. Shan, and T. F. Heinz, "Atomically thin MoS_2: a new direct-gap semiconductor," *Phys. Rev. Lett.*, vol. 105, 2010, Art no. 136805. https://doi.org/10.1103/PhysRevLett.105.136805.

[6] M. Koperski, K. Nogajewski, A. Arora, J. Marcus, K. Piotr, and M. Potemski, "Single photon emitters in exfoliated WSe_2 structures," *Nat. Nanotechnol.*, vol. 10, pp. 503–506, 2015, https://doi.org/10.1038/nnano.2015.67.

[7] H. J. Chuang, X. Tan, N. J. Ghimire, et al. "High mobility WSe2 p- and n-type field-effect transistors contacted by highly doped graphene for low-resistance contacts," *Nano Lett.,* vol. 14, pp. 3594–3601, 2014, 10.1021/nl501275p.

[8] W. Choi, M. Y. Cho, A. Konar, et al. "High-detectivity multilayer MoS2 phototransistors with spectral response from ultraviolet to infrared," *Adv. Mater.*, vol. 24, pp. 5832–5836, 2012, https://doi.org/10.1002/adma.201201909.

[9] O. Lopez-Sanchez, D. Lembke, M. Kayci, A. Radenovic, and A. Kis. "Ultrasensitive photodetectors based on monolayer MoS2," *Nat. Nanotechnol.*, vol. 8, pp. 497–501, 2013, https://doi.org/10.1038/nnano.2013.100.

[10] B. W. Baugher, H. O. Churchill, Y. Yang, and P. Jarillo-Herrero. "Optoelectronic devices based on electrically tunable p–n diodes in a monolayer dichalcogenide," *Nat. Nanotechnol.*, vol. 9, pp. 262–267, 2014, https://doi.org/10.1038/nnano.2014.25.

[11] A. Splendiani, L. Sun, Y. Zhang, et al., "Emerging photoluminescence in monolayer MoS2," *Nano Lett.,* vol. 10, pp. 1271–1275, 2010, https://doi.org/10.1021/nl903868w.

[12] M. Amani, D. Lien, D. Kiriya, et al., "Near-unity photoluminescence quantum yield in MoS2," *Science*, vol. 350, pp. 6264–6268, 2015. https://doi.org/10.1126/science.aad2114.

[13] N. Engheta, "Circuits with light at nanoscales: optical nanocircuits inspired by metamaterials," *Science*, vol. 317, pp. 1698–1702, 2007, 10.1126/science.1133268.

[14] S. Mei, K. Huang, H. Liu, et al., "On-chip discrimination of orbital angular momentum of light with plasmonic nanoslits," *Nanoscale*, vol. 8, pp. 2227–2233, 2016. https://doi.org/10.1039/C5NR07374J.

[15] D. Hu, Y. Lu, Y. Cao, et al., "Laser-splashed three-dimensional plasmonic nanovolcanoes for steganography in angular anisotropy," *ACS Nano*, vol. 12, pp. 9233–9239, 2018, https://doi.org/10.1021/acsnano.8b03964.

[16] B. Radisavljevic, and A. Kis, "Mobility engineering and a metal–insulator transition in monolayer MoS2," *Nat. Mater.*, vol. 12, pp. 815–820, 2013, https://doi.org/10.1038/nmat3687.

[17] F. Qin, L. Ding, L. Zhang, et al., "Hybrid bilayer plasmonic metasurface efficiently manipulates visible light," *Sci. Adv.*, vol. 2, 2016, Art no. e1501168, https://doi.org/10.1126/sciadv.1501168.

[18] Y. Cui, I. Y. Phang, R. S. Hegde, Y. H. Lee, H. K. Lee, and X. Y. Ling, "Encoding molecular information in plasmonic nanostructures for anti-counterfeiting applications," *Nanoscale*, vol. 1, pp. 631–637, 2014. https://doi.org/10.1039/C3NR04375D.

[19] K. C. Lee, Y.-H. Chen, H.-Y. Lin, et al., "Plasmonic gold nanorods coverage influence on enhancement of the photoluminescence of two-dimensional MoS2 monolayer," *Sci. Rep.*, vol. 5, 2015, Art no. 16374, https://doi.org/10.1038/srep16374.

[20] D. Liu, L. Yu, X. Xiong, et al., "Improving the luminescence enhancement of hybrid Au nanoparticle-monolayer MoS2 by focusing radially-polarized beams," *Opt. Express*, vol. 24, pp. 27554–27562, 2016, https://doi.org/10.1364/OE.24.027554.

[21] Z. Jia, H. Wei, D. Pan, and H. Xu, "Direction-resolved radiation from polarization-controlled surface plasmon modes on silver nanowire antennas," *Nanoscale*, vol. 8, pp. 20118–20124, 2016, 10.1039/C6NR07242A.

[22] C. Lumdee, B. Yun, and P. G. Kik, "Wide-band spectral control of Au nanoparticle plasmon resonances on a thermally and chemically robust sensing platform," *J. Phys. Chem. C.*, vol. 117, pp. 19127–19133, 2013, https://doi.org/10.1021/jp4056522.

[23] G.-C. Li, Q. Zhang, S. A. Maier, and D. Lei, "Plasmonic particle-on-film nanocavities: a versatile platform for plasmon-enhanced spectroscopy and photochemistry," *Nanophotonics*, vol. 7, pp. 1865–1889, 2018, https://doi.org/10.1515/nanoph-2018-0162.

[24] A. Tittl, X. Yin, H. Giessen, et al., "Plasmonic smart dust for probing local chemical reactions," *Nano Lett.,* vol. 13, pp. 1816–1821, 2013, https://doi.org/10.1021/nl4005089.

[25] R. Chikkaraddy, B. De Nijs, F. Benz, et al., "Single-molecule strong coupling at room temperature in plasmonic nanocavities," *Nature*, vol. 535, pp. 127–130, 2016, 10.1038/nature17974.

[26] D. Zheng, S. Zhang, Q. Deng, M. Kang, P. Nordlander, and H. Xu, "Manipulating coherent plasmon–exciton interaction in a single silver nanorod on monolayer WSe2," *Nano Lett.,* vol. 17, pp. 3809–3814, 2017, https://doi.org/10.1021/acs.nanolett.7b01176.

[27] R. T. Hill, J. J. Mock, Y. Urzhumov, et al., "Leveraging nanoscale plasmonic modes to achieve reproducible enhancement of light," *Nano Lett.*, vol. 10, pp. 4150–4154, 2010, https://doi.org/10.1021/nl102443p.

[28] S. Mubeen, S. Zhang, N. Kim, et al., "Plasmonic properties of gold nanoparticles separated from a gold mirror by an ultrathin oxide," *Nano Lett.,* vol. 12, pp. 2088–2094, 2012, https://doi.org/10.1021/nl300351j.

[29] L. Li, T. Hutter, U. Steiner, and S. Mahajan, "Single molecule SERS and detection of biomolecules with single gold nanoparticle on mirror junctions," *Analyst*, vol. 138, pp. 4574–4578, 2013, https://doi.org/10.1039/c3an00447c.

[30] Q. Zhang, G. Li, T. Lo, and D. Lei, "Polarization-resolved optical response of plasmonic particle-on-film nanocavities," *J. Opt.*, vol. 20, 2018, Art no. 024010, 10.1088/2040-8986/aaa1bc.

[31] R. Chikkaraddy, X. Zheng, F. Benz, et al., "How ultranarrow gap symmetries control plasmonic nanocavity modes: from cubes to spheres in the nanoparticle-on-mirror," *ACS Photon.*, vol. 4, pp. 469–475, 2017, https://doi.org/10.1021/acsphotonics.6b00908.

[32] X. Chen, Y. Yang, Y.-H. Chen, M. Qiu, R. J. Blaikie, and B. Ding, "Probing plasmonic gap resonances between gold nanorods and a metallic surface," *Phys. Chem. C.*, vol. 119, pp. 18627–18634, 2015, https://doi.org/10.1021/acs.jpcc.5b06006.

[33] G. M. Akselrod, C. Argyropoulos, T. B. Hoang, et al., "Probing the mechanisms of large Purcell enhancement in plasmonic nanoantennas," *Nat. Photonics*, vol. 8, pp. 835–840, 2014, https://doi.org/10.1038/nphoton.2014.228.

[34] H. Sugimoto, S. Yashima, M. Fujii, "Broadband dielectric–metal hybrid nanoantenna: silicon nanoparticle on a mirror," *ACS Photonics*, vol. 5, pp. 3421–3427, 2018. https://doi.org/10.1021/acsphotonics.7b01461.

[35] U. Bhanu, M. R. Islam, L. Tetard, and S. I. Khondaker, "Photoluminescence quenching in gold - MoS2 hybrid nanoflakes," *Sci. Rep.*, vol. 4, 2014, Art no. 5575, https://doi.org/10.1038/srep05575.

[36] R. Faggiani, J. Yang, and P. Lalanne, "Quenching, plasmonic, and radiative decays in nanogap emitting devices," *ACS Photon.*, vol. 2, pp. 1739–1744, 2015, https://doi.org/10.1021/acsphotonics.5b00424.

[37] C. Lee, H. Yan, L. E. Brus, et al., "Anomalous lattice vibrations of single- and few-layer MoS_2," *ACS Nano*, vol. 4, pp. 2695–2700, 2010, https://doi.org/10.1021/nn1003937.

[38] X. Liu, D. Y. Lei, "Simultaneous excitation and emission enhancements in upconversion luminescence using plasmonic double-resonant gold nanorods," *Sci. Rep.*, vol. 5, 2015, Art no. 15235, https://doi.org/10.1038/srep15235.

[39] P. B. Johnson, and R. W. Christy, "Turnability of the plasmonic response of the gold nanoparticles in infrared region," *Phys. Rev. B*, vol. 6, pp. 4370–4379, 1972.

[40] A. M.V an Der Zande, P. Y. Huang, D. A. Chenet, et al., "Grains and grain boundaries in highly crystalline monolayer molybdenum disulphide," *Nat. Mater.*, 12, pp. 554, 2013, https://doi.org/10.1038/nmat3633.

[41] S. Najmaei, Z. Liu, W. Zhou, et al., "Vapour phase growth and grain boundary structure of molybdenum disulphide atomic layers," *Nat. Mater.*, vol. 12, pp. 754, 2013, https://doi.org/10.1038/nmat3673.

[42] X. Wang, H. Feng, Y. Wu, and L. Jiao. "Controlled synthesis of highly crystalline MoS2 flakes by chemical vapor deposition," *J. Am. Chem. Soc.*, vol. 135, pp. 5304–5307, 2013, https://doi.org/10.1021/ja4013485.

[43] S. Tongay, W. Fan, J. Kang, et al., "Tuning interlayer coupling in large-area heterostructures with CVD-grown M.oS2 and WS2 monolayers," *Nano Lett.*, vol. 14, pp. 3185–3190, 2014, https://doi.org/10.1021/nl500515q.

[44] W. Gao, Y. H. Lee, R. Jiang, J. Wang, T. Liu, and X. Y. Ling, "Localized and continuous tuning of monolayer MoS2 photoluminescence using a single shape-controlled Ag nanoantenna," *Adv. Mater.*, vol. 4, pp. 701–706, 2016, https://doi.org/10.1002/adma.201503905.

[45] T. W. Lo, Q. Zhang, M. Qiu, et al., "Thermal redistribution of exciton population in monolayer transition metal dichalcogenides probed with plasmon–exciton coupling spectroscopy," *ACS Photon.*, vol. 6, pp. 411–421, 2019, https://doi.org/10.1021/acsphotonics.8b01349.

[46] K. Park, T. Jiang, G. Clark, X. Xu, and M. B. Raschke, "Radiative control of dark excitons at room temperature by nano-optical antenna-tip Purcell effect," *Nat. Nanotechnol.*, vol. 13, pp. 59–64, 2018, https://doi.org/10.1038/s41565-017-0003-0.

[47] Y. Zhou, G. Scuri, D. Wild, et al., "Probing dark excitons in atomically thin semiconductors via near-field coupling to surface plasmon polaritons," *Nat. Nanotechnol.*, vol. 12, pp. 856–860, 2017, https://doi.org/10.1038/nnano.2017.106.

[48] G. Wang, C. Robert, M. M. Glazov, et al., "In-plane propagation of light in transition metal dichalcogenide monolayers: optical

selection rules," *Phys. Rev. Lett.*, vol. 119, Art no. 047401, 2017, https://doi.org/10.1103/PhysRevLett.119.047401.

[49] C. T. Yip, T. W. Lo, S. Zhu, et al., "Tight-binding modeling of excitonic response in van Der Waals stacked 2D semiconductors," *Nanoscale Horiz.*, vol. 4, pp. 969–974, 2019, 10.1039/C9NH00042A.

[50] W. Chen, S. Zhang, M. Kang, et al., "Probing the limits of plasmonic enhancement using a two-dimensional atomic crystal probe," *Light: Sci. Appl.*, vol. 7, pp. 56, 2018, 10.1038/s41377-018-0056-3.

[51] G.-C. Li, Y.-L. Zhang, J. Jiang, Y. Luo, and D. Y. Lei, "Metal-substrate-mediated plasmon hybridization in a nanoparticle dimer for photoluminescence line-width shrinking and intensity enhancement," *ACS Nano*, vol. 11, pp. 3067–3080, 2017, https://doi.org/10.1021/acsnano.7b00048.

[52] Y. Zhao, X. Liu, D. Y. Lei, and Y. Chai, "Effects of surface roughness of Ag thin films on surface-enhanced Raman spectroscopy of graphene: spatial nonlocality and physisorption strain," *Nanoscale*, vol. 6, pp. 1311–1317, 2014, https://doi.org/10.1039/c3nr05303b.

[53] Z. Xie, Y. Duo, Z. Lin, et al., "The rise of 2D photothermal materials beyond graphene for clean water production," *Adv. Sci.*, vol. 7, 2020, Art no. 1902236. https://doi.org/10.1002/advs.201902236.

[54] Z. J. Xie, C. Y. Xing, W. Huang, et al., "Ultrathin 2D nonlayered tellurium nanosheets: facile liquid-phase exfoliation, characterization, and photoresponse with high performance and enhanced stability," *Adv. Funct. Mater.*, vol. 28, 2018, Art no. 1705833, 10.1002/adfm.201705833.

[55] C. Ma, J. Yan, Y. Huang, C. Wang, and G. Yang, "The optical duality of tellurium nanoparticles for broadband solar energy harvesting and efficient photothermal conversion," *Sci. Adv.*, vol. 4, Art no. eaas9894, 2018, https://doi.org/10.1126/sciadv.aas9894.

Supplementary Material: The online version of this article offers supplementary material (https://doi.org/10.1515/nanoph-2020-0178).